Title

Optimal boundary control of a model thin-film fiber coating model



Authors

Biswal, Shiba

Ji, Hangjie

Elamvazhuthi, Karthik

et al.

Publication Date

2024

DOI

10.1016/j.physd.2023.133942

Peer reviewed

# Optimal Boundary Control of a Model Thin-Film Fiber Coating Model ⋆

Shiba Biswal[a,1,*], Hangjie Ji[b,2], Karthik Elamvazhuthi[c], Andrea L. Bertozzi[d]

[a] *University of California, Los Angeles, Department of Mathematics, Los Angeles, 90095, California, USA*
[b] *North Carolina State University, Department of Mathematics, Raleigh, 27695, North Carolina, USA*
[c] *University of California, Riverside, Department of Mechanical Engineering, Riverside, 92521, California, USA*
[d] *University of California, Los Angeles, Department of Mathematics and Mechanical and Aerospace Engineering, Los Angeles, 90095, California, USA*

**Abstract**

This paper considers the control of fluid on a solid vertical fiber, where the fiber radius is larger than the film thickness. The fluid dynamics is governed by a fourth-order partial differential equation (PDE) that models this flow regime. Fiber coating is affected by the Rayleigh-Plateau instability that leads to breakup into moving droplets. In this work, we show that control of the film profile can be achieved by dynamically altering the input flux to the fluid system that appears as a boundary condition of the PDE. We use the optimal control methodology to compute the control function. This method entails solving a minimization of a given cost function over a time horizon. We formally derive the optimal control conditions, and numerically verify that subject to the domain length constraint, the thin film equation can be controlled to generate a desired film profile with a single point of actuation. Specifically, we show that the system can be driven to both constant film

⋆The MATLAB code and data is publicly available at https://github.com/ShibaBiswal/Optimal-Boundary-Control-for-Thin-Film-Equation-

*Corresponding author

*Email addresses:* sbiswal@math.ucla.edu (Shiba Biswal), hangjie_ji@ncsu.edu (Hangjie Ji ), kelamvazhuthi@engr.ucr.edu (Karthik Elamvazhuthi), bertozzi@math.ucla.edu (Andrea L. Bertozzi)

[1]SB was supported by Simons Math + X Investigator Award number 510776.

[2]HJ was supported by NSF grant DMS 2309774.

profiles and traveling waves of certain speeds.

*Keywords:* Thin-film Equation, Optimal Control, Boundary Control, PDE Control, Distributed Parameter Systems

---

## 1. Introduction

Thin viscous liquid films flowing down vertical cylindrical fibers exhibit complex and interesting interfacial dynamics. Driven by the Rayleigh-Plateau instability, the liquid films form droplets or pulses that flow down along the fiber. The flow dynamics depend on the flow rate, fiber radius, liquid properties, and inlet conditions [14]. These factors can lead to stable trains of droplets that behave like a traveling wave, droplet coalescence, and isolated moving droplets separated by small amplitude waves [12, 9]. For applications of such coating flows in particle capture [25], desalination [33, 26], and other mass and heat exchangers [34, 32], it is crucial to maintain a stable film profile with desired characteristics.

Classical lubrication theory is widely studied for thin liquid films flowing down vertical fibers at small flow rates. In the thin film limit where the characteristic liquid film thickness is significantly smaller than the fiber radius, the leading-order evolution equation for the film thickness $h$, derived by Trifonov [30] and Frenkel [10], and further studied by [4, 15], is given by

$$h_t + \left[\delta h^3 \left(h_x + h_{xxx}\right) + \tfrac{2}{3} h^3\right]_x = 0. \tag{1}$$

Here, $\delta = 2l_c^2 h_0/(3R^3)$ measures the ratio of curvature-driven flow to the gravity driven mean flow, where $l_c = (\sigma/\rho g)^{1/2}$ is the capillary wave length, $\rho$ is the fluid density, $g$ is the gravitational acceleration, $\sigma$ is the surface tension, and $h_0$ is the thickness of the initial flat film that is taken to be the characteristic film height. The higher-order term $h_{xxx}$ corresponds to the stabilizing streamwise surface tension, $h_x$ represents the destabilizing azimuthal curvature, and the last term $\frac{2}{3}h^3$ represents gravity. We note that equation (1) is a simplified fiber coating model that contains linearized curvatures terms and neglects the geometric contribution of the substrate. More classical models for fiber coating dynamics that incorporate substrate geometry, slip length, moderate inertia and fully-nonlinear curvatures have been developed and investigated in [7, 12, 24, 23, 22, 14].

Introducing a change of scaling $t \to t/\delta$ to equation (1) leads to an equivalent model for the film thickness $h(t,x)$ over a domain $0 \le x \le L$,

$$h_t + \left[h^3\left(G + h_x + h_{xxx}\right)\right]_x = 0, \tag{2}$$

where the Bond number $G = 2/(3\delta) = (\rho g R^3)/(\sigma h_0)$. This is a nonlinear fourth-order parabolic type partial differential equation, where $h^3$ represents the mobility function, and the Bond number $G$ plays a significant role in the solution dynamics. Based on the analysis in [4, 15], given the (initial) average film thickness $h_0 = 1$, traveling pulses that move steadily at constant speeds exist for $G$ smaller than a critical $G_* \approx 0.6$. More recently, Halpern and Wei also investigated slip-enhanced drop formation [11] using a variant of equation (2) that incorporates the Navier-slip condition.

In this paper, we aim to control the coating film solution profiles in (2) by controlling the inlet flux at $x = 0$, $q(t,0)$, where the flux is given by,

$$q(t,x) = h^3(G + h_x + h_{xxx}). \tag{3}$$

This is motivated by recent experimental and analytical studies [14, 27] that reveal the importance of the inlet geometry and flow rate to the downstream droplet dynamics. Interesting experimental work for the nonlinear response of the fiber coating dynamics to periodic forcing at the inlet has also been presented in [8]. The authors showed that the spatial response of the downstream dynamics strongly depends on the ratio of the forcing frequency to a critical frequency corresponding to the maximum linear growth rate. Following the work in [14, 13], we impose the following Dirichlet boundary conditions $h(t,0) = h_{in}, q(t,0) = u(t)$ at the inlet, where the inlet flux $q(t,0)$ appears as a boundary condition of the PDE that governs the evolution of the film thickness. At the outlet $x = L$, we impose the Neumann boundary conditions $h_x(t,L) = h_{xxx}(t,L) = 0$. We show via numerical studies that the equation (2) can be controlled to maintain nearly-constant film thickness and desired travelling waves, subject to constraints.

Expanding equation (2) around a flat film state, $h(t,x) \sim 1 + \hat{h}(t,x)$, where $\hat{h}(t,x) \ll 1$, we obtain a weakly nonlinear equation,

$$\hat{h}_t + 3G\hat{h}_x + 6G\hat{h}\hat{h}_x + \hat{h}_{xx} + \hat{h}_{xxxx} = 0.$$

Using the rescaling $\hat{h} \to (6G)^{-1}\hat{h}$ and a change of coordinates $x \to x - 3Gt$ in the moving reference frame, this equation can be transformed to the classical

Kuramoto-Sivashinsky (KS) equation [15],

$$\hat{h}_t + \hat{h}\hat{h}_x + \hat{h}_{xx} + \hat{h}_{xxxx} = 0. \tag{4}$$

A significant amount of research exists on the control of the KS equation (4). A well-studied approach to controlling this PDE is to obtain a finite-dimensional approximation a reduced-order-model (ROM) that captures the dominant dynamics of the PDE, and then apply standard control methodologies to this ROM. For example, some earlier works proposed a distributed control (one that acts on the whole domain) for the KS equation under periodic boundary conditions [2, 5, 18]. Another approach to controlling the KS equation is through its boundary term, either the Neumann boundary condition, or the Dirichlet boundary condition. For example, in [16] the linear KS equation is reduced to an equivalent finite dimensional system using the Sturm-Liouville decomposition, and then controlled through its boundary. However, unlike ordinary differential equations, in the case of PDEs, local linear stability may not necessarily imply local nonlinear stability. In the case of KS equation, conditions that guarantee this implication are provided in [1]. A few researchers [19, 6, 20] have also shown boundary control of nonlinear KS equation which does not rely on discretization of the PDE is possible. Optimal control of the KS equation is studied in [29]. The literature on control of the full nonlinear thin-film equation, of the type that we consider in this paper, is very limited. In [17], the authors consider an optimal control of a thin-film type equation that only contains the fourth-order derivative. In [28], for a thin film evolving on a plane without any gravitational effect, a linear proportional control for the suppression of the Marangoni instability has been explored. To the best of our knowledge, control of the thin film equation (2) that we consider in this paper has not been studied.

The paper is organized as follows. In Section 2 we formulate the optimal control problem. The details of the derivation are provided in Appendix 5. We verify the algorithm via numerical simulations presented in Section 3. Section 4 shows concluding remarks of this paper.

## 2. Optimal Control Formulation

In this section we introduce and formulate the optimal control problem. We begin by defining the notations, and restating the thin-film equation (2) with its imposed boundary conditions.

We denote the non-dimensional fiber length by $L$. The state space is denoted by $\Omega = [0, L]$. The symbol $\partial\Omega$ stands for the boundary of $\Omega$. At any given time $t$ and $x \in \Omega$, we let $h(t, x)$ denote the fluid thickness across the fiber length. The flux, denoted by $q$, is given by (3). In this paper, we set the input flux, $q(t, 0)$, to be the time-dependent scalar-valued control parameter $u(t)$.

Consider the one-dimensional PDE (2) again now with its boundary and initial conditions. The system evolves on $[0, T] \times \Omega$.

$$h_t + \left(h^3(G + h_x + h_{xxx})\right)_x = 0$$

$$q(t, 0) = \left(h^3(G + h_x + h_{xxx})\right)\big|_{(x=0)} = u(t), \tag{5}$$

$$h(t, 0) = h_{in}, \quad h_x(t, L) = 0, \quad h_{xxx}(t, L) = 0 \tag{6}$$

$$h(0, x) = h_0 \tag{7}$$

Here, $h_{in} > 0$ is a fixed scalar.

Our goal is to design a $u(t)$ such that the film profile $h(t, x)$ is close to a desired fluid profile $h^d(t, x)$, in a given finite time $T \in (0, \infty)$, in the $L^2([0, T], \Omega)$ sense. Due to $T$ being chosen to be finite, this choice of control methodology is called the finite-horizon optimal control problem. In this work, we consider $h^d$ to be both a film of constant thickness and a traveling wave. In the case of traveling wave profiles $h^d$, we use the periodic boundary condition as opposed to the one outlined above in (5)-(6), the details are provided in the numerical section 3.2. Furthermore, we require that the $(L^2([0, T]))$ norm of control $u(t)$ to be bounded. Therefore, we consider the following objective function,

$$J(h, u) = \frac{1}{2}\int_0^T \|h(t, x) - h^d(t, x)\|^2_{L^2(\Omega)} dt + \frac{\lambda}{2}\|u(t)\|^2_{L^2([0,T])}. \tag{8}$$

Here, $\lambda > 0$ is a weighting parameter of choice.

The optimal control problem is posed as a constrained minimization problem of the above cost function (8), over a set of controls $U = \{u(t) : 0 \leq u(t) \leq u_p\}$, subject to the PDE (2) and its boundary conditions (6). Here, $u_p$ is an upper bound for the control. The lower bound is constrained to be zero, since in our application the input flux, which is necessarily non-negative, is chosen to be the control function. Therefore, the optimal control problem can be stated as follows:

**Problem 2.1.**

$$\min_{u\in U} J(h,u) = \frac{1}{2}\int_0^T \|h(t,x) - h^d(t,x)\|^2_{L^2(\Omega)} dt + \frac{\lambda}{2}\|u(t)\|^2_{L^2([0,T])} \qquad (9)$$

*subject to,*

$$\begin{aligned}
&h_t + (h^3(G + h_x + h_{xxx}))_x = 0 \ \textit{in}\ [0,T]\times\Omega \\
&(h^3(G + h_x + h_{xxx}))\big|_{(x=0)} - u(t) = 0, \\
&h(t,0) - h_{in} = 0, \quad h_x(t,L) = 0, \quad h_{xxx}(t,L) = 0 \\
&h(0,x) = h_0
\end{aligned}$$

*and*

$$0 \le u(t) \le u_p \ \textit{for a.e. } t.$$

We will use *gradient descent* to find a solution to the optimization problem. However, we note that the cost function (8) is a function of two variables $h$ and $u$. However, algorithmically, gradient descent is difficult to implement for this optimization problem due to the PDE constraints. To get around this problem, it is standard in the optimal control literature to treat $h$ as a variable dependent on $u$ via the PDE constraint (5). This will enable us to perform gradient descent on the variable $u$ rather than both $h$ and $u$. Towards this goal, we define the *reduced objective functional* $f : U \to \mathbb{R}$ by $f(u) = J(h(u), u)$ for all $u \in U$, where $h(u)$ is the solution of the equation (2)-(7) for a given $u$. In terms of the reduced objective functional, the optimal control problem 2.1 can alternatively expressed as

**Problem 2.2.**

$$\inf_{u\in U} f(u)$$

While one can compute the gradient of the function $f(u)$, with respect to u, using the finite difference method, this approach is not numerically tractable since $u(t)$ is a function. Alternatively, one can compute the gradient of $f(u)$ using the *formal Lagrange method* [31] or the method of Lagrange multipliers to the optimization problem 2.1. This method leads to a numerically tractable expression for this gradient using the so called *adjoint equation*. While the method leads to the formulation of the correct expression for the gradient, the derivation of the conditions is not mathematically rigorous. This is because applying this method to optimization problems

with PDE constraints requires addressing additional technicalities, such as the existence of solutions and the differentiability of the objective functional. These technicalities are outside the scope of this paper. We will use the method formally to derive the first order necessary conditions of optimality and provide numerical evidence that this thin film equation can be controlled for certain short lengths using an optimal control approach.

We will now eliminate the constraint equations by means of Lagrange multipliers, $p_1(t,x)$, $p_2(t)$, $p_3(t)$, $p_4(t)$, $p_5(t)$. The multipliers are grouped into a vector $p = [p_1, p_2, p_3, p_4, p_5]$. To this end, we define the Lagrangian function,

$$\begin{aligned}\mathcal{L}(h,u,p) = J(h,u) &- \int_0^T \int_\Omega p_1(t,x)\left(h_t + \left(h^3(G + h_x + h_{xxx})\right)_x\right) dx\ dt \\ &- \int_0^T p_2(t)\left((h^3(G + h_x + h_{xxx}))|_{(x=0)} - u(t)\right) dt \\ &- \int_0^T p_3(t)(h(t,0) - h_{in})dt - \int_0^T p_4(t)h_x(t,L)dt \\ &- \int_0^T p_5(t)h_{xxx}(t,L)dt.\end{aligned}$$

Let $\bar{h}, \bar{u}$ denote the optimal values of $h(t,x)$ and $u(t)$ respectively. Moreover, we will assume that $\bar{h}$ is strictly positive on $[0,L]$; as will be seen later in Section 5, this assumption will prove to be necessary in deriving the optimality conditions. First-order necessity condition requires that the derivative of $\mathcal{L}$ with respect to $h$ must vanish at the optimal point $(\bar{h}, \bar{u})$, that is,

$$D_h\mathcal{L}(\bar{h}, \bar{u}, p)v = 0,\ \forall v \text{ s.t. } v(0,x) = 0. \tag{10}$$

The condition $v(0,x) = 0$ imposed above on the perturbation $v$ is to ensure that the initial condition (7) is fixed. This necessary condition yields the following adjoint equation and the corresponding boundary conditions. Details

of the derivation have been provided in the Appendix 5.

$$-(p_1)_t - (\bar{h} - h^d) + (p_1)_x(3\bar{h}^2(G + \bar{h}_x + \bar{h}_{xxx})) - \left((p_1)_x\bar{h}^3\right)_x - \left((p_1)_x\bar{h}^3\right)_{xxx} = 0 \text{ in } \Omega \tag{11}$$

$$(p_1)_x(t,0) = 0, \tag{12}$$

$$(p_1)_{xx}(t,0) = 0 \tag{13}$$

$$(p_1)_x(t,L) = 0 \tag{14}$$

$$-p_1(t,L) + (p_1)_{xxx}(t,L) = 0 \tag{15}$$

$$p_1(T,x) = 0 \tag{16}$$

The adjoint equation is solved backward in time, hence the condition (16) is the initial condition for the adjoint equation. The initial condition set to zero here follows from equation (33) (in Appendix).

The gradient of the reduced objective functional $f(u)$ with respect to $u$ can be computed using the gradient of the Lagrangian [31] as

$$f_u(u) = D_u\mathcal{L}(h,u,p). \tag{17}$$

From the constraints on $u$, we deduce that the optimal control $\bar{u}$ must satisfy the following variational inequality,

$$D_u\mathcal{L}(\bar{h},\bar{u},p)(u-\bar{u}) = \int_0^T (\lambda\bar{u} + \bar{p_2})(u-\bar{u}) \geq 0, \ \forall u \in U \tag{18}$$

To find $(\bar{h},\bar{u})$, we perform gradient descent on the optimization problem using the expression for the gradient in (17). The system (2)-(6) is solved forward in time $t \in [0,T]$, hence it is called the *forward equation*. As previously mentioned, the adjoint equation (11)-(15) is solved backward in time $\tau = T - t \in [0,T]$, hence it is referred to as the *backward equation*. The search for an optimal control entails performing a gradient descent on $u$. The algorithm is presented in Algorithm 1. Statements 9 – 11 in Algorithm 1 implement the *projected gradient method* [3]. This ensures that the obtained $u$ is strictly non-negative. Moreover, we let $u(t)$ be unbounded as this choice does not lead to any algorithm convergence issues.

## 3. Numerical Studies

To simulate the thin-film equation (2) and its adjoint equation (11) with their respective boundary conditions, (5)-(6), (12)-(15), we use finite-difference

**Algorithm 1** Gradient Descent

**Input**: $h^d(t,x), \lambda, \Delta, n, T$ ▷ $\Delta$:= Step size, $n$:= Number of iterations
**Initialize** $h(t=0,x), p_1(t=T,x), u_0(t)$ ▷ $u_0(t)$:=Initial guess for the control law
Solve for $h(t,x)$ in (2)-(7), with (5) set to $u_0(t)$.
Compute the initial cost $L_0$ (8) with $h(t,x)$, $u_0(t)$
**for** $i = 1 : n$ **do**
    Solve for $p_1$ in (11)-(15), with $\bar{h}(t,x)$ set to $h(t,x)$.
    Set $p_2(t) = p_1(t, x=0)$ (see (32))
    Compute $u_c(t) = u_{i-1}(t) - \Delta(\lambda u_{i-1}(t) + p_2(t))$.
    **if** $u_c(t_j) < 0$ for some $t_j \in [0,T]$ **then** ▷ Projected Gradient
        Set $u_c(t_j) = 0$
    **end if**
    Solve for $h_c(t,x)$ in (2) -(6), with (5) set to $u_c(t)$
    Compute cost $L_i$ with $h_c(t,x)$, $u_c(t)$
    **if** $L_i < L_{i-1}$ **then**
        $u_i(t) = u_c(t)$
        $h(t,x) = h_c(t,x)$
    **else**
        Set $\Delta = \Delta/2$
    **end if**
**end for**

method for space discretization. In particular, we choose a uniform grid and use second-order of accuracy. This results in a $N$-dimension ordinary differential equation (ODE) in time. The ODE obtained is simulated in *Matlab*, using the *ode15s* solver, a variable-step, variable-order solver based on the numerical differentiation formulas (NDFs) of orders 1 to 5. The necessity of this solver arises due to the stiffness of the system.

We test the optimal control design in two settings: in Section 3.1, the desired profile $h^d$ is set to be a constant function, and in Section 3.2, $h^d$ is set to be a traveling wave of given speed. In the examples presented next, we make the following choices of initial conditions and parameters. The initial condition for the forward equation (2) is set to be a near constant function $h_0$, such that the integral of $h_0$ over $[0, L]$ is close to the integral of $h^d$. If not chosen this way, the optimization algorithm fails to converge to a solution. If the initial condition $h_0$ is not chosen in this way, the optimization algorithm may fail to converge to a solution. This may be due to the infeasibility of the resulting optimization problem when the initial condition of the PDE is far away from the desired configuration. In such a situation, we say that the control system is not *globally controllable*. The control is initialized to be a strictly positive constant function $u_0$. The weighting parameter $\lambda$ in (8) is set at 1. We choose the values of $u_0$, final time $T$, and step size $\Delta$ specific to the example.

### *3.1. Spatially-Uniform Solutions*

We begin by discussing the stability of spatially-uniform profiles for (2) under periodic boundary conditions. Although, these results do not translate to the boundary conditions that we consider (5)-(6), we expect that these results hold for the subdomain away from the inlet and outlet boundary at $x = 0, L$. Consider a spatially-uniform film $h(t, x) = \bar{h}$ over a periodic domain $[0, l]$, perturbed by an infinitesimal Fourier mode,

$$h = \tilde{h} + \varepsilon e^{\mathrm{i}(kx - \Lambda t)}. \tag{19}$$

Here, $k = 2\pi\hat{k}/l$ is the wave number, $\hat{k} = 1, 2, \cdots$ represents the number of waves in the perturbation, $\Lambda$ is the wave frequency, and $\varepsilon \ll 1$ is the initial amplitude. Substituting this expression into (2), and linearizing around the base state $\tilde{h}$ yields the dispersion relation,

$$\Lambda = 3G\tilde{h}k + \mathrm{i}\tilde{h}^3k^2(1 - k^2), \tag{20}$$

where $c = 3G\tilde{h}$ is the speed of linear kinematic wave solutions of (2) for small wave numbers. The form (20) indicates that the second-order azimuthal curvature term $(h^3 h_x)_x$ is destabilizing, and the fourth-order streamwise surface tension $(h^3 h_{xxx})_x$ term is stabilizing. When the effective growth rate $\mathrm{Im}(\Lambda)$ is greater than 0, the spatial perturbation grows in time and the flat film $\tilde{h}$ becomes long-wave unstable with respect to any wave number $0 < k < 1$. Alternatively, choosing $\hat{k} = 1$, (20) shows that for any domain size $l > 2\pi$, the flat film is linearly unstable.

Next, we consider the steady state solution $\tilde{h}(x)$ of the model (2) subject to the inlet and outlet boundary conditions (5)–(6). By setting the time derivative term $h_t = 0$ in (2) and integrating once, we obtain the third-order ODE for the steady state solution $\tilde{h}(x)$,

$$\frac{d^3\tilde{h}}{dx^3} + \frac{d\tilde{h}}{dx} = \frac{u}{\tilde{h}^3} - G, \tag{21}$$

subject to the boundary conditions

$$\tilde{h}(0) = h_{in}, \quad \tilde{h}_x(L) = \tilde{h}_{xxx}(L) = 0. \tag{22}$$

In the absence of active control, we assume that the boundary control is constant in time, $u(t) \equiv u_0$. This ODE is similar to the one studied in [21] that models the meniscus structures of a surface-tension driven liquid films. Since $\tilde{h}(x)$ satisfies the boundary conditions $\tilde{h}_x(L) = \tilde{h}_{xxx}(L) = 0$, (21) yields the relation $\tilde{h}(L) = (u_0/G)^{1/3}$. Therefore, the steady-state flat film solution $\tilde{h} \equiv h_{in}$ of (2) only exists if the control $u_0$ satisfies $u_0 = h_{in}^3 G$. A non-trivial steady state solution for the boundary value problem (21)-(22) is determined by the Bond number $G$, the inlet film thickness $h_{in}$, and the flux $u_0$. By setting the derivative terms $d^3\tilde{h}/dx^3 = d\tilde{h}/dx = 0$ in (21), the asymptotic behavior of a typical nontrivial steady state satisfies

$$\tilde{h} \to (u_0/G)^{1/3} \quad \text{for } x \to L. \tag{23}$$

Alternatively, to obtain a steady state solution of a desired flat film thickness $h \to h^d$ away from the inlet, the boundary flux control $u_0$ should satisfy

$$u_0 \sim G(h^d)^3. \tag{24}$$

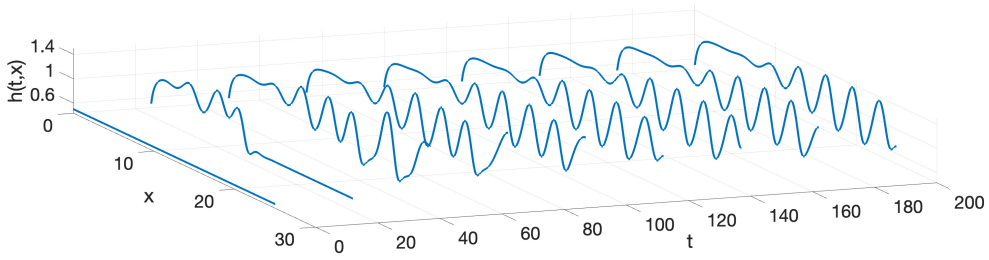


(a) Simulation of uncontrolled $h(t,x)$, with $u_0 = 0.5$

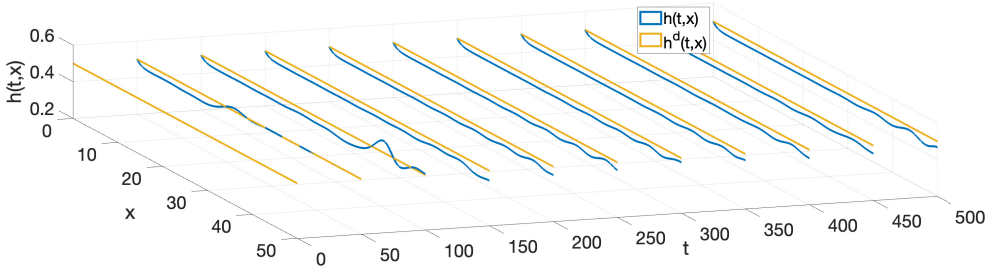


(b) Simulation of controlled $h(t,x)$ against the desired traveling wave profile $h^d = 0.5$

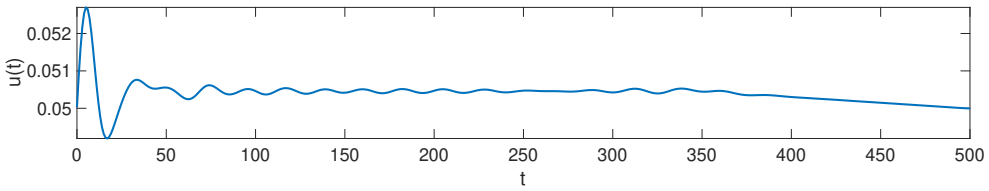


(c) Corresponding $u(t)$ obtained from the optimal control algorithm

Figure 1: Simulation from Example 1 on a domain size $L = 50$, with $G = 0.5$ and $h_0 = 0.5$

*3.1.1. Example 1*

In view of the discussion above, we consider the optimal control Problem 2.1 with a spatially constant desired profile on a domain of length $L > 2\pi$. Specifically, we consider a desired profile $h^d(t, x) = 0.5$ on a domain of size $L = 50$ and set the Bond number $G = 0.5$. Due to the input flux, the relatively long domain, and low Bond number, the Rayleigh-Plateau instability dominates the system, and the uniform film breaks into ripples. This spatial instability is numerically shown in the simulation of the uncontrolled system (2) in Figure 1(a). Starting from a spatially-uniform initial condition $h_0 = 0.5$ in (7), the sequential plots of $h(t, x)$ in Figure 1(a) show the evolution of the PDE solution to the uncontrolled system (2), where the input flux (5) is set to a (time-invariant) constant function $u = u_0 \equiv 0.5$. Driven by the Rayleigh-Plateau instability, the solution develops a wavy pattern away from the inlet.

We apply the optimal control Algorithm 1 to this example for a final time $T = 500$. Identical initial condition $h_0 = 0.5$ is used for the forward equation as in the uncontrolled case. Figure 1(b) shows the simulation of the forward equation (2) with the boundary control (5) set to the control $u(t)$ obtained from the algorithm. The control $u$, in time, is shown in Figure 1(c). We observe that the controlled system does not break into ripples and converges to approximately $h \approx 0.47$ away from the inlet, close to the desired flat film $h^d = 0.5$. Numerical simulation suggests that this observed $h$, that forms a meniscus like profile starting from 0.5 and converges to 0.47, is locally stable. The optimal control algorithm appears to converge to this nontrivial equilibrium. Moreover, we observe that the average value of $u$ is 0.05, which is close to $u_0 \sim 0.0625$ predicted by the formula (24) for $G = 0.5$ and $h^d \equiv 0.5$. While we do not expect the Rayleigh-Plateau instability to dominate under this low average value of input flux $u_0 \sim 0.05$, nonetheless, this example provides us with evidence that the optimal control algorithm results in an output that is verifiable against the analytical result obtained in (24). Moreover, the need to design such control laws is better appreciated in the upcoming sections wherein we will let the desired film profile be traveling waves.

*3.2. Traveling Wave Solutions*

In this section, we let the desired fluid profile $h^d$ to be a chosen traveling wave. We generate these traveling waves by considering (2) over a periodic domain $x \in [0, L]$ with boundary conditions $h^d(t, x) = h^d(t, x+L)$. The PDE

has traveling wave solutions that take the form,

$$h^d(t,x) = H(\xi), \qquad \xi = x - ct, \tag{25}$$

where $c$ is the speed of the traveling wave. Substituting the ansatz (25) into (2) yields a fourth-order nonlinear ordinary differential equation for $H(\xi)$,

$$-cH_\xi + \left[H^3\left(G + H_\xi + H_{\xi\xi\xi}\right)\right]_\xi = 0. \tag{26}$$

This is a nonlinear eigenvalue problem for the traveling wave profile $H$ and the speed $c$. We apply Newton's method to solve the equation (26), where $c$ is treated as an unknown. Following the numerical method used in [12], we impose a constraint on mass conservation as follows. To achieve local uniqueness of the solution, define

$$M_0 = \int_0^L H(\xi)\, d\xi, \tag{27}$$

and set $H(\xi_0) = H_0$, for some $0 \le \xi_0 \le L$. Applying the *numerical continuation method* to the system yields a family of traveling wave solutions $H(\xi; M_0, L)$ of (26) and (27), parameterized by paired parameters $(M_0, L)$.

We note that the traveling waves $H(\xi)$ do not necessarily satisfy the boundary conditions (5)–(6). In fact, for liquid flowing down a vertical cylindrical fibers, the dynamics of the flow near the inlet and outlet strongly depend on the boundary conditions [14]. For droplet dynamics in the Rayleigh-Plateau regime where a steady train of droplets travel down the fiber with nearly constant speed and spacing, one may approximate the flow dynamics away from the inlet and outlet by traveling waves [12]. In this work, we will use traveling wave solutions $H(\xi)$ associated with periodic boundary conditions as desired solution profiles in the control problem.

*3.2.1. Example 2: Slow Traveling Waves*

As a first example, we numerically generate a relatively 'slow' traveling wave $H(\xi)$ over a periodic domain of size $L = 10$. This was achieved by solving the traveling wave ODE (26) subject to the constraint (27) with the mass $M_0 = 3.622$ and the Bond number $G = 0.5$. The generated traveling wave is associated with a relatively slow speed $c = 0.2$, and its evolution in time $h^d(t,x) = H(x - ct)$ is shown in orange in Figure 2(a). We verify numerically that the one-period traveling wave $H(\xi)$ is stable over the domain $0 \le \xi \le L$ with respect to perturbations of the same period. A detailed stability analysis of traveling waves in similar thin film models can be found in [12].

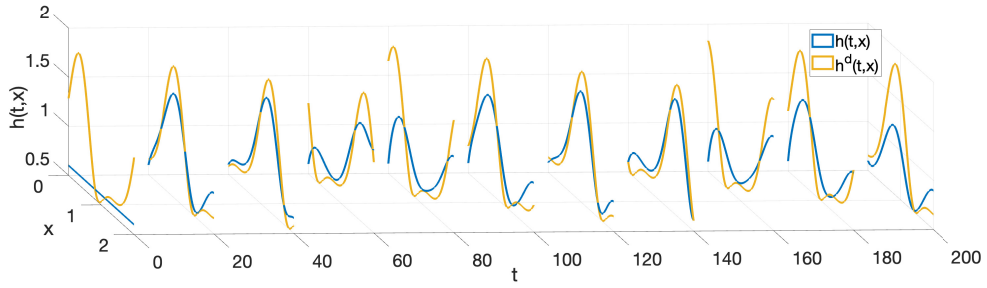


(a) Simulation of controlled $h(t,x)$ against the desired traveling wave profile $h^d(t,x)$.

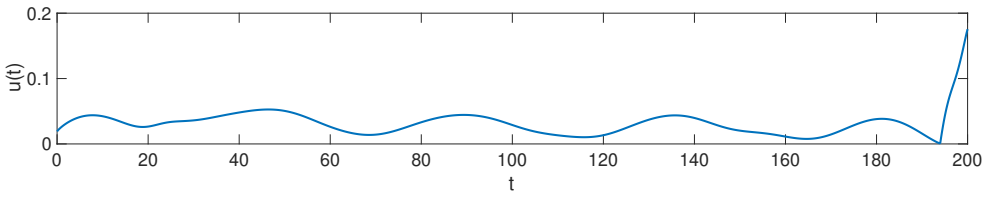


(b) Corresponding $u(t)$ obtained from the optimal control algorithm.

Figure 2: Simulation from Example 2 on domain size $L = 10$, with $G = 0.5$ and $M_0 = 3.622$.

We choose the initial condition for the forward equation (2) to be the constant function $h_0 = 0.4$. The optimal control algorithm was run for $T = 200$, which corresponds to 4 cycles of the wave traveling over the domain $[0, L]$. The boundary control function $u(t)$ obtained from the algorithm is presented in Figure 2(b). As expected, we observe that the control $u$ shows periodicity; moreover, it appears to achieve a steady state type of behavior away from $t = T$. We simulate the solution of (2) after substituting the $u$ obtained from the algorithm in (5). Figure 2(a) shows the snapshots of time and spatial evolution of the solution $h(t,x)$. Figure 3 shows the $L^2([0,T],\Omega)$ error between $h$ and $h^d$ against the number of iterations. From the figures presented we observe that the film thickness $h$ indeed converges approximately to $h^d$. In general, on short domains, the

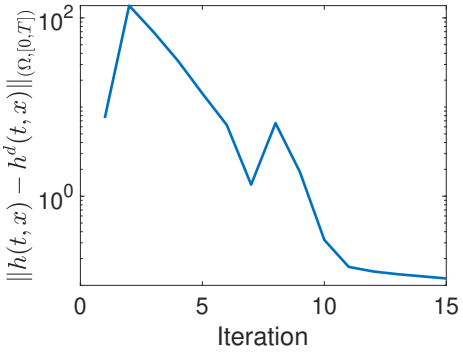


Figure 3: Logarithm of the cost function (8), with $\lambda = 0$, evaluated in Example 2, corresponding to Figure 2a, against iterations.

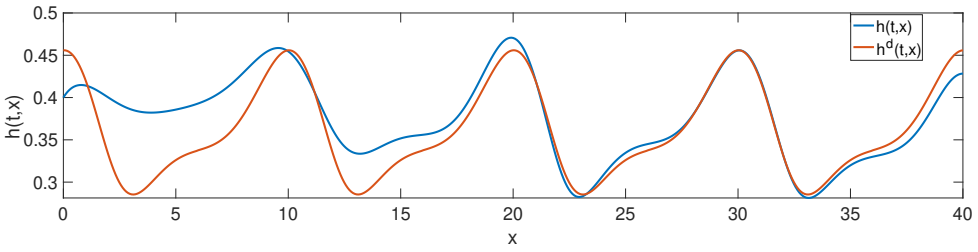


(a) Snapshot at $t = 180$, over $L = 40$

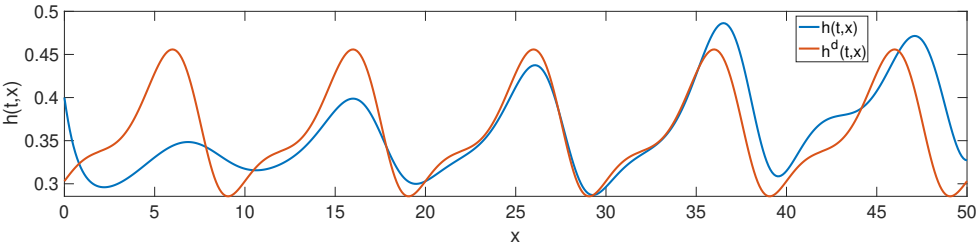


(b) Snapshot at $t = 260$, over $L = 50$

Figure 4: Simulation of the controlled $h(t, x)$ against the desired traveling wave profile $h^d(t, x)$ at specific time instants $t$, over different domain sizes $L$, with $G = 0.5$. The profile $h^d$ in each case is obtained by replicating the $h^d$ from Example 2 (shown in Figure 2a) over $L$.

fluid film converges to a uniform film, however, this example serves as numerical evidence that active control can be used to make the fluid film break into ripples.

To test our algorithm on long domains, we duplicate the desired traveling wave $h^d$ (shown in Figure 2(a)) over integral multiples of $L = 10$. Specifically, duplicating over $L = 40$ produces a train of 4 droplets, and over $L = 50$, produces a train of 5 droplets. Both are shown in red at an arbitrary time instant $t$ in Figure 4(a) and 4(b), respectively. Our numerical study shows that these periodic multi-pulse traveling waves are unstable under periodic boundary conditions. Perturbing these multi-pulse traveling waves over the periodic domain $0 \leq x \leq L$ leads the dynamic solution to the PDE (2) produce irregular wavy patterns in long-time simulations. However, using the optimal control algorithm, we are able to design a boundary control that generates consistent PDE solutions that resemble the desired traveling waves. In the former case, i.e. $L = 40$, the algorithm was run for $T = 200$. In the latter case, $L = 50$, the final time was set at $T = 300$. In both cases, the initial condition of the forward equation is set at $h_0 = 0.4$. Figures 4(a) and 4(b) show snapshots of the space evolution of the controlled $h$ at $t = 180$ and $t = 260$, respectively. We observe that in both these cases, the optimal control algorithm is able to find a $u$ that drives the system (2) close to the desired wave profile $h^d$, away from the boundary.

*3.2.2. Example 3: Fast Traveling Waves*

In this example, we generate a 'fast' traveling wave on $L = 10$. Similar to the previous case, this was achieved by solving (26) subject to the constraints (27) over a periodic domain. In this case, we let $M_0 = 10.088$, and $G = 0.5$. The traveling wave obtained has a speed $c = 1.652$, and its evolution in time is shown in orange in Figure 5(a). The initial condition of the forward equation (7) is set at $h_0 = 0.6$. The optimal control $u(t)$ generated in this case, obtained for $T = 200$, is presented in 5(b).

Figure 6 shows the $L^2([0, T], \Omega)$ error between $h(t, x)$ and $h^d(t, x)$. Here we observe that the error is significantly higher than in Example 2. This can also be noted from the $h$ simulation in Figure 5(a), we observe that although the controlled $h$ is able to match $h^d$ in frequency, it fails to do so in amplitude. We believe that this is because in Example 2 the wave speed, $c = 0.2$, is slower than this example's wave speed, $c = 1.652$. There appears to be a limitation on the speed of the traveling wave that prohibits reaching this solution $h^d$ exactly. This indicates that the set of reachable states from

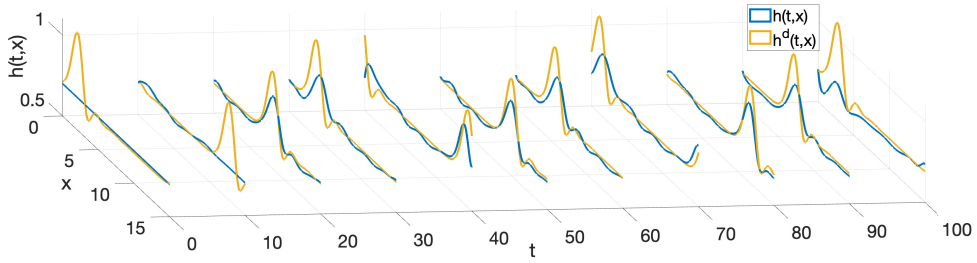


(a) Simulation of controlled $h(t, x)$ against the desired traveling wave profile $h^d(t, x)$.

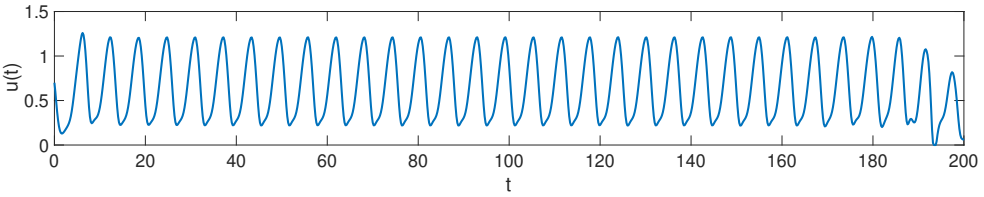


(b) Corresponding $u(t)$ obtained from the optimal control algorithm.

Figure 5: Simulation from Example 3 on domain size $L = 10$, with $G = 0.5$ and $M_0 = 10.088$.

a given initial condition does not necessarily include all film profiles.

Furthermore, we extend the domain from $L = 10$ to 40 and duplicate the $h^d$ profile from Figure 5(a) to obtain a train of 4 pulses. Similar to Example 2 discussed in Section 3.2, the single pulse traveling wave $h^d(\xi)$ considered in this example is stable over a periodic domain, while the 4-pulse traveling wave is unstable. The simulated controlled $h(t, x)$ is shown in Figure 7 at time instant $t = 54$. However, in this case, we observe that the algorithm is not able to find a control $u$ that makes the system converge to $h^d$. This is unlike in Example 2 where an optimal control is found for longer domains. This could be attributed potentially to the higher speed of the traveling wave. Without a full controllability analysis, it appears that the algorithm

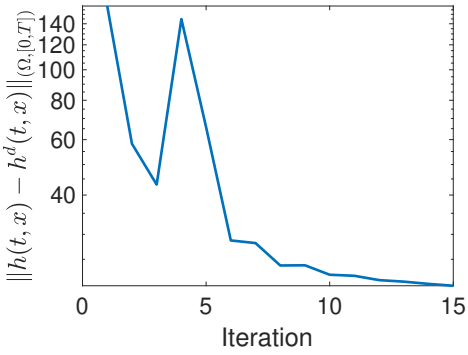


Figure 6: Logarithm of the cost function (8), with $\lambda = 0$, evaluated in Example 3 corresponding to 5a, against iterations

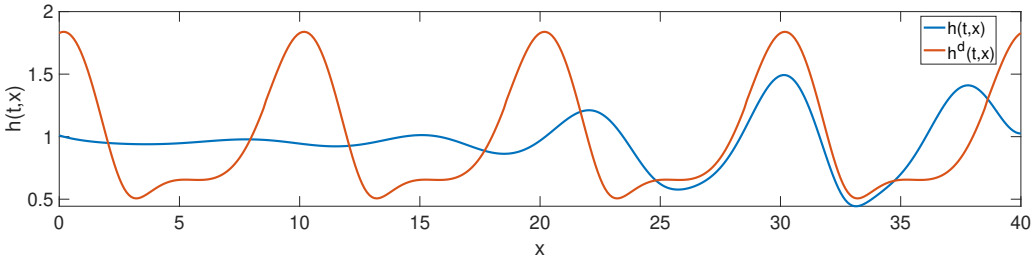


Figure 7: Simulation of the controlled $h(t,x)$ against the desired traveling wave profile $h^d(t,x)$ at specific time instant $t = 54$, over $L = 40$, with $G = 0.5$. The profile $h^d$ in is obtained by replicating the $h^d$ from Example 3 (shown in Figure 5a) over $L$.

works better for slow traveling waves or short domains.

*3.2.3. Example 4: Isolated Pulse with Large Inter-Pulse Spacing*

As our final example, we generate a traveling wave $h^d(t,x)$ that has a higher speed on a long domain, as compared to Example 3. Similar to the previous cases, $h^d$ is generated by solving the traveling wave ODE (26) under periodic boundary conditions over a domain of size $L = 30$ with the mass constraint $M_0 = 22$ and the Bond number $G = 1$. This results in an unstable traveling wave of speed $c = 2.13$. PDE simulation of equation (2) starting from this isolated pulse with a small perturbation yields a transition into a train of two-pulse traveling wave over the periodic domain. Snapshots of the spatial evolution of desired wave profile are shown in orange in Figure 8(a). The optimal control found in this case is presented in Figure 8(b). Snapshots of the corresponding solution $h(t,x)$ are presented in Figure 8(a). Although, we expect that with a large Bond number $G = 1$ over a short domain of size $L = 30$, the fluid film will converge to a uniform film away from the inlet, under the action of active control, the system is able to track the desired traveling closely.

Similar to previous cases, we duplicated the $h^d$, presented in 8(a), to obtain two pulses over $L = 60$. Figure 9 shows the simulation of the controlled $h$ at a time step $t = 170$. We observe that, although the speed is much higher in this case, the system is able to track $h^d$ very closely, unlike in the case of Figure 7. We believe this could be attributed to the fact that in this case, the frequency of $h^d$, due to higher inter-pulse spacing, is smaller than the case in 7.

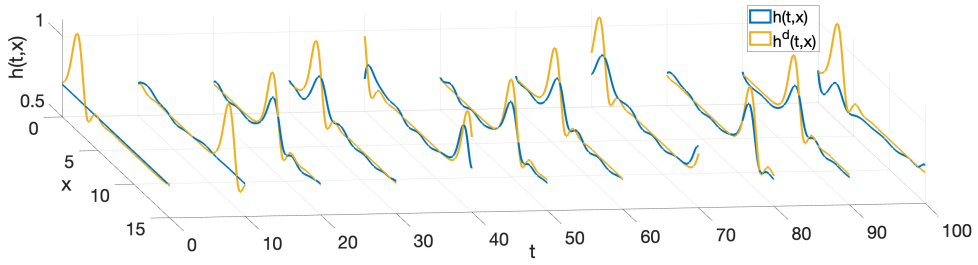


(a) Simulation of controlled $h(t,x)$ against the desired traveling wave profile $h^d(t,x)$.

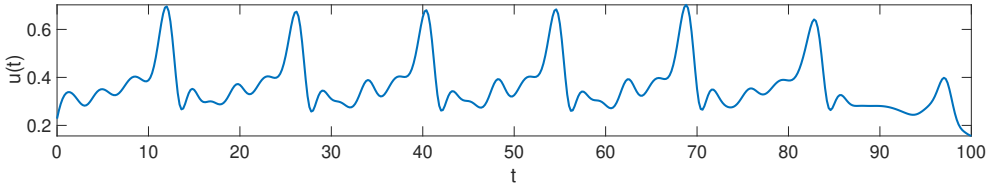


(b) Corresponding $u(t)$ obtained from the optimal control algorithm.

Figure 8: Simulation from Example 4 on domain size $L = 30$, with $G = 1$ and $M_0 = 22$.

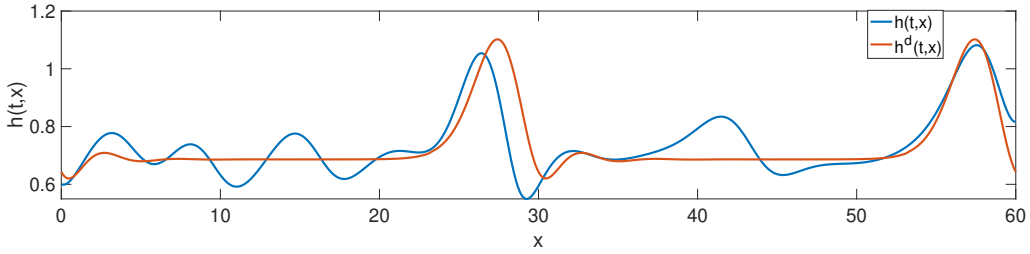


Figure 9: Simulation of the controlled $h(t,x)$ against the desired traveling wave profile $h^d(t,x)$ at specific time instant $t = 170$, over $L = 60$, with $G = 1$. The profile $h^d$ in is obtained by replicating the $h^d$ from Example 3 (shown in Figure 8a) over $L$.

## 4. Conclusion

Our goal in this work is to present a proof-of-concept that the nonlinear thin-film equation, considered in this paper, can be controlled to both constant and traveling wave profiles of small wave speeds, over short domain sizes. Specifically, with respect to the uniform film profile case, we are able to design (time-dependent) control laws such that the controlled system converges to a uniform film on a domain size where the Rayleigh-Plateau instability is not very significant. With regards to general traveling waves, the controlled system is able to converge to a slow traveling wave on relatively long domain of size up to $L = 50$. For relatively fast traveling waves of high frequency on short domains, the optimal control algorithm generates a control function that matches the traveling wave in frequency, and not in amplitude. However, the algorithm does generate a control law that is able to track fast traveling waves of low frequency on long domains closely. In conclusion, the numerical experiments seem to indicate that the thin-film equation under the given boundary conditions is controllable for certain domain sizes, and for initial conditions $h_{in}$, that are close to $h^d$ in the $L^2(\cdot)$ sense. Our study also highlights the limitations of boundary control. Future work will investigate the possibility of numerically characterizing the controllability properties of the system and designing stabilizing feedback controllers. A stabilizing control law can potentially render a desired film profile locally asymptotically stable.

## 5. Appendix

We provide the details of derivation of the adjoint equation in this section. Expanding the LHS of (10) we obtain the following

$$
\begin{aligned}
D_h\mathcal{L}(\bar{h},\bar{u},\bar{p_i})v = &\int_0^T\int_\Omega(\bar{h}-h^d)v \\
&-\int_0^T\int_\Omega p_1\left\{v_t+\left(3\bar{h}^2v+(3\bar{h}^2\bar{h}_xv+\bar{h}^3v_x)+(3\bar{h}^2\bar{h}_{xxx}v+\bar{h}^3v_{xxx})\right)_x\right\} \\
&-\int_0^T p_2\{\left(3\bar{h}^2v+(3\bar{h}^2\bar{h}_xv+\bar{h}^3v_x)+(3\bar{h}^2\bar{h}_{xxx}v+\bar{h}^3v_{xxx})\right)\Big|_{x=0}-u\} \\
&-\int_0^T p_3v(0,t)-\int_0^T p_4v_x(L,t)-\int_0^T p_5v_{xxx}(L,t)
\end{aligned}
$$

Applying integration by parts,

$$
\begin{aligned}
D_h\mathcal{L}(\bar{h},\bar{u},\bar{p_i})v = &\int_0^T\int_\Omega(\bar{h}-h^d)v - \int_\Omega(p_1v)\Big|_0^T + \int_0^T\int_\Omega(p_1)_tv \\
&- \int_0^T(p_1 3\bar{h}^2v)\Big|_{\partial\Omega} + \int_0^T\int_\Omega(p_1)_x(3\bar{h}^2v) \\
&- \int_0^T(p_1(3\bar{h}^2\bar{h}_xv+\bar{h}^3v_x))\Big|_{\partial\Omega} + \int_0^T\int_\Omega(p_1)_x(3\bar{h}^2\bar{h}_xv+\bar{h}^3v_x) \\
&- \int_0^T(p_1(3\bar{h}^2\bar{h}_{xxx}v+\bar{h}^3v_{xxx}))\Big|_{\partial\Omega} + \int_0^T\int_\Omega(p_1)_x(3\bar{h}^2\bar{h}_{xxx}v+\bar{h}^3v_{xxx}) \\
&- \int_0^T p_2\{\big(3\bar{h}^2v+(3\bar{h}^2\bar{h}_xv+\bar{h}^3v_x)+(3\bar{h}^2\bar{h}_{xxx}v+\bar{h}^3v_{xxx})\big)\Big|_{x=0} - u\} \\
&- \int_0^T p_3v(0,t) - \int_0^T p_4v_x(L,t) - \int_0^T p_5v_{xxx}(L,t)
\end{aligned}
$$

Applying integration by parts once more,

$$
\begin{aligned}
D_h\mathcal{L}(\bar{h},\bar{u},\bar{p_i})v = &\int_0^T\int_\Omega(\bar{h}-h^d)v - \int_\Omega(p_1v)\Big|_0^T + \int_0^T\int_\Omega(p_1)_tv \\
&- \int_0^T p_1(3\bar{h}^2v)\Big|_{\partial\Omega} + \int_0^T\int_\Omega(p_1)_x(3\bar{h}^2v) - \int_0^T(p_1(3\bar{h}^2\bar{h}_xv+\bar{h}^3v_x))\Big|_{\partial\Omega} \\
&+ \int_0^T\int_\Omega(p_1)_x(3\bar{h}^2\bar{h}_xv) + \int_0^T((p_1)_x\bar{h}^3v)\Big|_{\partial\Omega} - \int_0^T\int_\Omega\left((p_1)_x\bar{h}^3\right)_x v \\
&- \int_0^T(p_1(3\bar{h}^2\bar{h}_{xxx}v+\bar{h}^3v_{xxx}))\Big|_{\partial\Omega} + \int_0^T\int_\Omega(p_1)_x(3\bar{h}^2\bar{h}_{xxx}v) \\
&+ \int_0^T\left((p_1)_x\bar{h}^3v_{xx}\right)\Big|_{\partial\Omega} - \int_0^T\left(\left((p_1)_x\bar{h}^3\right)_x v_x\right)\Big|_{\partial\Omega} + \int_0^T\left(\left((p_1)_x\bar{h}^3\right)_{xx} v\right)\Big|_{\partial\Omega} \\
&- \int_0^T\int_\Omega\left((p_1)_x\bar{h}^3\right)_{xxx} v \\
&- \int_0^T p_2(t)\{\big(3\bar{h}^2v+(3\bar{h}^2\bar{h}_xv+\bar{h}^3v_x)+(3\bar{h}^2\bar{h}_{xxx}v+\bar{h}^3v_{xxx})\big)\Big|_{x=0} - u\} \\
&- \int_0^T p_3(t)v(0,t) - \int_0^T p_4(t)v_x(L,t) - \int_0^T p_5(t)v_{xxx}(L,t)
\end{aligned}
$$

Since $D_h\mathcal{L}(\bar{h},\bar{u},\bar{p_i})v = 0$ for all perturbations $v$, choose a subset of $v(t,x)$ such that $v = v_x = v_{xx} = v_{xxx} = 0$ at $x = 0, L$, and $v = 0$ at $t = 0, T$. Then

$D_h\mathcal{L}(\bar{h},\bar{u},p)v = 0$ yields,

$$D_h\mathcal{L}(\bar{h},\bar{u},p)v = \int_0^T\int_\Omega(\bar{h}-h^d)v + \int_0^T\int_\Omega(p_1)_t v + \int_0^T\int_\Omega(p_1)_x(3\bar{h}^2 v)$$
$$+\int_0^T\int_\Omega(p_1)_x(3\bar{h}^2\bar{h}_x v) - \int_0^T\int_\Omega\left((p_1)_x\bar{h}^3\right)_x v$$
$$+\int_0^T\int_\Omega(p_1)_x(3\bar{h}^2\bar{h}_{xxx} v) - \int_0^T\int_\Omega\left((p_1)_x\bar{h}^3\right)_{xxx} v = 0.$$

This implies that,

$$(p_1)_t + (\bar{h}-h^d) + 3(p_1)_x\bar{h}^2 + 3(p_1)_x\bar{h}^2\bar{h}_x - \left((p_1)_x\bar{h}^3\right)_x$$
$$+3(p_1)_x\bar{h}^2\bar{h}_{xxx} - \left((p_1)_x\bar{h}^3\right)_{xxx} = 0.$$

The equation above can be rewritten to obtain the adjoint equation (11).

Next, choose $v$ such that $v_x = v_{xx} = v_{xxx} = 0$ at $x = 0$, and $v = 0$ at $t = 0, T$, then $D_h\mathcal{L}(\bar{h},\bar{u},\bar{p_i})v = 0$ implies that,

$$-\int_0^T p_1 3\bar{h}^2 v\Big|_{x=0} - \int_0^T (p_1 3\bar{h}^2\bar{h}_x v)\Big|_{x=0} + \int_0^T ((p_1)_x\bar{h}^3 v)\Big|_{x=0}$$
$$-\int_0^T (p_1 3\bar{h}^2\bar{h}_{xxx} v)\Big|_{x=0} + \int_0^T \left(\left((p_1)_x\bar{h}^3\right)_{xx} v\right)\Big|_{x=0}$$
$$-\int_0^T p_2(t)\left(3\bar{h}^2 v + 3\bar{h}^2\bar{h}_x v + 3\bar{h}^2\bar{h}_{xxx} v\right)\Big|_{x=0} - \int_0^T p_3 v(0,t) = 0.$$

This further implies that,

$$\Big(-p_1(3\bar{h}^2)(1+\bar{h}_x+\bar{h}_{xxx}) + (p_1)_x\bar{h}^3 + ((p_1)_x\bar{h}^3)_{xx}$$
$$-p_2(3\bar{h}^2)(1+\bar{h}_x+\bar{h}_{xxx})\Big)\Big|_{x=0} = p_3. \tag{28}$$

Proceeding similarly, choose $v$ such that $v_x = v_{xx} = v_{xxx} = 0$ at $x = L$, and $v = 0$ at $t = 0, T$, then $D_h\mathcal{L}(\bar{h},\bar{u},\bar{p_i})v = 0$ implies that,

$$\left(-p_1(3\bar{h}^2)(1+\bar{h}_x+\bar{h}_{xxx}) + (p_1)_x\ \bar{h}^3 + ((p_1)_x\bar{h}^3)_{xx}\right)\Big|_{x=L} = 0. \tag{29}$$

Continuing, choose $v$ such that $v = v_{xx} = v_{xxx} = 0$ at $x = 0$ , and $v = 0$ at $t = 0, T$. Then $D_h\mathcal{L}(\bar{h},\bar{u},\bar{p_i})v = 0$ yields,

$$\left(-p_1\bar{h}^3 - ((p_1)_x\bar{h}^3)_x - p_2\bar{h}^3\right)\Big|_{x=0} = 0. \tag{30}$$

Choose $v$ such that $v = v_{xx} = v_{xxx} = 0$ at $x = L$, and $v = 0$ at $t = 0, T$. Then $D_h\mathcal{L}(\bar{h}, \bar{u}, \bar{p_i})v = 0$ yields,

$$(-p_1\bar{h}^3 - ((p_1)_x\ \bar{h}^3)_x)\Big|_{x=L} = p_4. \tag{31}$$

Choose $v$ such that $v = v_x = v_{xxx} = 0$ at $x = 0$, and $v = 0$ at $t = 0, T$. Then $D_h\mathcal{L}(\bar{h}, \bar{u}, \bar{p_i})v = 0$ yields,

$$(p_1)_x\ \bar{h}^3\Big|_{x=0} = 0.$$

Since we have assumed that $\bar{h} > 0$, the above equation implies, $(p_1)_x\Big|_{(x=0)} = 0$, which gives us the first boundary condition (12) for $p_1$ at $x = 0$.

Choose $v$ such that $v = v_x = v_{xxx} = 0$ at $x = L$, and $v = 0$ at $t = 0, T$. Then, $D_h\mathcal{L}(\bar{h}, \bar{u}, \bar{p_i})v = 0$ implies,

$$(p_1)_x\ \bar{h}^3\Big|_{x=L} = 0.$$

Since we have assumed that $\bar{h} > 0$, the above equation further implies that $(p_1)_x(t, x)\Big|_{(x=L)} = 0$, which gives us the third boundary condition (14) for $p_1$ at $x = L$.

Choose $v$ such that $v = v_x = v_{xx} = 0$ at $x = 0$, and $v = 0$ at $t = 0, T$. Then $D_h\mathcal{L}(\bar{h}, \bar{u}, \bar{p_i})v = 0$ implies,

$$(-p_1\bar{h}^3 - p_2\bar{h}^3)\Big|_{x=0} = 0.$$

This equation further implies

$$p_2(t) = -p_1(0, t). \tag{32}$$

Choose $v$ such that $v = v_x = v_{xx} = 0$ at $x = L$, and $v = 0$ at $t = 0, T$. Then $D_h\mathcal{L}(\bar{h}, \bar{u}, \bar{p_i})v = 0$ yields an expression for the Lagrange multiplier $p_5(t)$,

$$p_5 = (-p_1\bar{h}^3)\Big|_{x=L}.$$

Finally, choosing $v$ such that $v = 0$ at $t = 0$ yields,

$$(p_1 v)\Big|_{t=T} = 0 \tag{33}$$

which yields the initial condition for the adjoint equation (16) $p_1(T, x) = 0$ .

Substituting (6), (14) in (29), we get the second boundary condition (15) for the adjoint equation at $x = L$, $(-p_1 + (p_1)_{xxx})\Big|_{x=L} = 0$. Similarly, substituting (32) and (12) in (30), gives us the second boundary condition (13) at $x = 0$, $(p_1)_{xx}\Big|_{x=0} = 0$. Substituting (14) in (31), we get an expression for the multiplier $p_4(t)$,

$$p_4 = \left(p_1\bar{h}^3 - (p_1)_{xx}\bar{h}^3\right)\Big|_{x=L}.$$

And finally, the expression for the Lagrange multiplier $p_3(t)$ can be obtained from (28); the expression can be simplified by substituting the boundary conditions (12)-(13).

## References


[1] Rasha Al Jamal and Kirsten Morris. Linearized stability of partial differential equations with application to stabilization of the kuramoto–sivashinsky equation. *SIAM Journal on Control and Optimization*, 56(1):120–147, 2018.

[2] Antonios Armaou and Panagiotis D Christofides. Feedback control of the kuramoto–sivashinsky equation. *Physica D: Nonlinear Phenomena*, 137(1-2):49–61, 2000.

[3] Stephen Boyd, Stephen P Boyd, and Lieven Vandenberghe. *Convex optimization*. Cambridge university press, 2004.

[4] Hsueh-Chia Chang and Evgeny A Demekhin. Mechanism for drop formation on a coated vertical fibre. *Journal of Fluid Mechanics*, 380:233–255, 1999.

[5] Panagiotis D Christofides and Antonios Armaou. Global stabilization of the kuramoto–sivashinsky equation via distributed output feedback control. *Systems & Control Letters*, 39(4):283–294, 2000.

[6] Jean-Michel Coron and Qi Lü. Fredholm transform and local rapid stabilization for a kuramoto–sivashinsky equation. *Journal of Differential Equations*, 259(8):3683–3729, 2015.

[7] R. V. Craster and O. K. Matar. On viscous beads flowing down a vertical fibre. *Journal of Fluid Mechanics*, 553:85–105, 2006.

[8] C. Duprat, C. Ruyer-Quil, and F. Giorgiutti-Dauphiné. Spatial evolution of a film flowing down a fiber. *Physics of Fluids*, 21(4):042109, 2009.

[9] C Duprat, C Ruyer-Quil, S Kalliadasis, and F Giorgiutti-Dauphiné. Absolute and convective instabilities of a viscous film flowing down a vertical fiber. *Physical review letters*, 98(24):244502, 2007.

[10] AL Frenkel. Nonlinear theory of strongly undulating thin films flowing down vertical cylinders. *EPL (Europhysics Letters)*, 18(7):583, 1992.

[11] David Halpern and Hsien-Hung Wei. Slip-enhanced drop formation in a liquid falling down a vertical fibre. *Journal of Fluid Mechanics*, 820:42–60, 2017.

[12] H. Ji, C. Falcon, A. Sadeghpour, Z. Zeng, Y. S. Ju, and A. L. Bertozzi. Dynamics of thin liquid films on vertical cylindrical fibres. *Journal of Fluid Mechanics*, 865:303–327, 2019.

[13] H. Ji, C. Falcon, E. Sedighi, A. Sadeghpour, Y. S. Ju, and A. L. Bertozzi. Thermally-driven coalescence in thin liquid film flowing down a fibre. *Journal of Fluid Mechanics*, 916, 2021.

[14] H Ji, A Sadeghpour, YS Ju, and AL Bertozzi. Modelling film flows down a fibre influenced by nozzle geometry. *Journal of Fluid Mechanics*, 901, 2020.

[15] Serafim Kalliadasis and Hsueh-Chia Chang. Drop formation during coating of vertical fibres. *Journal of Fluid Mechanics*, 261:135–168, 1994.

[16] Rami Katz and Emilia Fridman. Finite-dimensional control of the kuramoto-sivashinsky equation under point measurement and actuation. In *2020 59th IEEE Conference on Decision and Control (CDC)*, pages 4423–4428. IEEE, 2020.

[17] Markus Klein and Andreas Prohl. Optimal control for the thin film equation: Convergence of a multi-parameter approach to track state constraints avoiding degeneracies. *Computational Methods in Applied Mathematics*, 16(4):685–702, 2016.

[18] CH Lee and HT Tran. Reduced-order-based feedback control of the kuramoto–sivashinsky equation. *Journal of computational and applied mathematics*, 173(1):1–19, 2005.

[19] Wei-Jiu Liu and Miroslav Krstić. Stability enhancement by boundary control in the kuramoto–sivashinsky equation. *Nonlinear Analysis: Theory, Methods & Applications*, 43(4):485–507, 2001.

[20] Mohamed Maghenem, Christophe Prieur, and Emmanuel Witrant. Boundary control of the kuramoto-sivashinsky equation under intermittent data availability. In *American Control Conference*, 2022.

[21] Andreas Münch and PL Evans. Interaction of advancing fronts and meniscus profiles formed by surface-tension-gradient-driven liquid films. *SIAM Journal on Applied Mathematics*, 66(5):1610–1631, 2006.

[22] Yadong Ruan, Ali Nadim, Lekha Duvvoori, and Marina Chugunova. Liquid films falling down a vertical fiber: modeling, simulations and experiments. *Fluids*, 6(8):281, 2021.

[23] C Ruyer-Quil, P Treveleyan, F Giorgiutti-Dauphiné, C Duprat, and S Kalliadasis. Modelling film flows down a fibre. *Journal of Fluid Mechanics*, 603:431–462, 2008.

[24] C. Ruyer-Quil, S. P. M. J. Trevelyan, F. Giorgiutti-Dauphiné, C. Duprat, and S. Kalliadasis. Film flows down a fiber: Modeling and influence of streamwise viscous diffusion. *The European Physical Journal Special Topics*, 166(1):89–92, 2009.

[25] A. Sadeghpour, F. Oroumiyeh, Y. Zhu, D. D. Ko, H. Ji, A. L. Bertozzi, and Y. S. Ju. Experimental study of a string-based counterflow wet electrostatic precipitator for collection of fine and ultrafine particles. *Journal of the Air & Waste Management Association*, pages 1–15, 2021.

[26] A Sadeghpour, Z Zeng, H Ji, N Dehdari Ebrahimi, AL Bertozzi, and YS Ju. Water vapor capturing using an array of traveling liquid beads for desalination and water treatment. *Science advances*, 5(4):eaav7662, 2019.

[27] A. Sadeghpour, Z. Zeng, and Y. S. Ju. Effects of nozzle geometry on the fluid dynamics of thin liquid films flowing down vertical strings in the Rayleigh-Plateau regime. *Langmuir*, 33:6292–6299, 2017.

[28] Anna E Samoilova and Alexander Nepomnyashchy. Feedback control of marangoni convection in a thin film heated from below. *Journal of Fluid Mechanics*, 876:573–590, 2019.

[29] Ruben J Tomlin, Susana N Gomes, Grigorios A Pavliotis, and Demetrios T Papageorgiou. Optimal control of thin liquid films and transverse mode effects. *SIAM Journal on Applied Dynamical Systems*, 18(1):117–149, 2019.

[30] Yu Trifonov et al. Steady-state traveling waves on the surface of a viscous liquid film falling down on vertical wires and tubes. *AIChE journal*, 38(6):821–834, 1992.

[31] Fredi Tröltzsch. *Optimal control of partial differential equations: theory, methods, and applications*, volume 112. American Mathematical Soc., 2010.

[32] Z. Zeng, A. Sadeghpour, and Y. S. Ju. Thermohydraulic characteristics of a multi-string direct-contact heat exchanger. *International Journal of Heat and Mass Transfer*, 126:536–544, 2018.

[33] Z. Zeng, A. Sadeghpour, and Y. S. Ju. A highly effective multi-string humidifier with a low gas stream pressure drop for desalination. *Desalination*, 449:92–100, 2019.

[34] Z. Zeng, A. Sadeghpour, G. Warrier, and Y. S. Ju. Experimental study of heat transfer between thin liquid films flowing down a vertical string in the Rayleigh-Plateau instability regime and a counterflowing gas stream. *International Journal of Heat and Mass Transfer*, 108:830–840, 2017.